Electronic Supplementary Material (ESI) for Journal of Materials Chemistry A.

A room-temperature self-healing elastomer with ultra-high strength and toughness fabricated via optimized hierarchical hydrogen-bonding interactions

LiangLiang Xia, HongJun Tu, Wen Zeng, XiaoLing Yang, Ming Zhou*, Linkai Li, Xiao Guo

Liang Liang Xia, HongJun Tu, Wen Zeng, XiaoLing Yang
School of New Energy and Materials, Southwest Petroleum University, Chengdu, 610500, P. R. China

Ming Zhou, Linkai Li, Xiao Guo
State Key Laboratory of Oil and Gas Reservoir Geology and Exploitation, School of New Energy and Materials, Southwest Petroleum University, Chengdu, 610500, P. R. China

*Corresponding author. E-mail: mr.zhouming@163.com

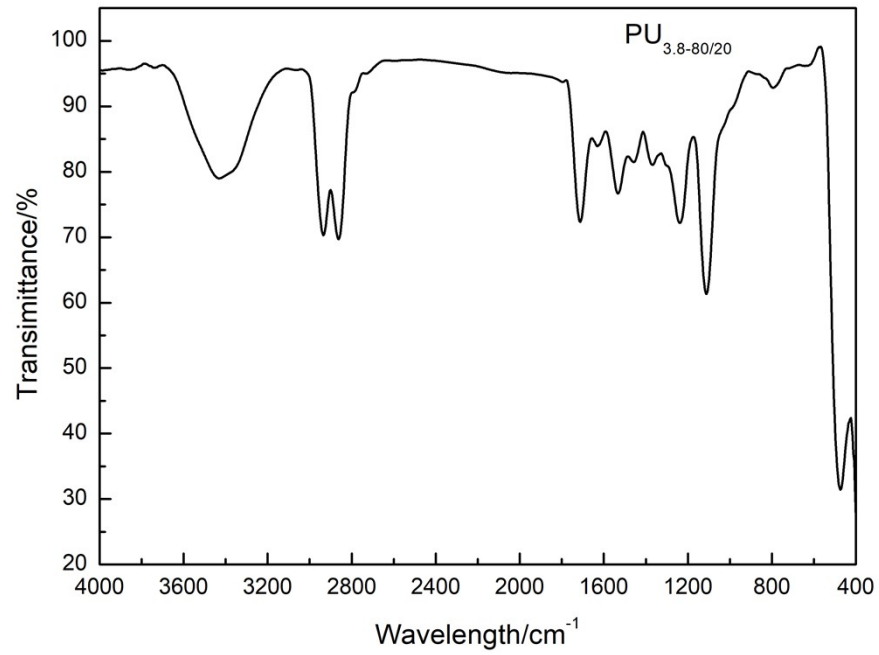

Figure S1. FTIR spectrum of $PU_{3.8\text{-}80/20}$.

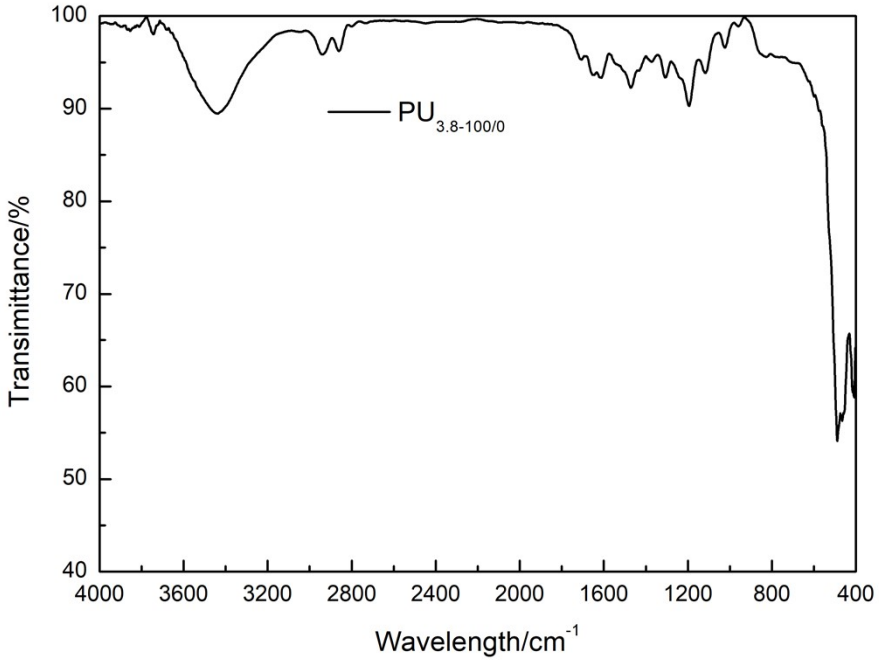

Figure S2. FTIR spectrum of $PU_{3.8\text{-}100/0}$.

Table S1. FT-IR characteristic peak assignments of $PU_{3.8\text{-}80/20}$.

Assignments	Wavenumber(cm^{-1})
H-bonded ν (N-H)	3428.9
νa (CH_2)	2935
νs (CH_2)	2854
H-bonded ν (C=O) amide	1712
H-bonded ν (C-N) + δ (N-H) amide	1531
H-bonded ν (C-N) + δ (N-H) amide	1234
ν (C-O-C)	1114
δ (-C_7H_5-)	794

Table S2. FT-IR characteristic peak assignments of $PU_{3.8\text{-}100/0}$.

Assignments	Wavenumber(cm^{-1})
H-bonded ν (N-H)	3442
νa (CH_2)	2946
νs (CH_2)	2869
H-bonded ν (C=O) amide	1716
H-bonded ν (C-N) + δ (N-H) amide	1481
H-bonded ν (C-N) + δ (N-H) amide	1201
ν (C-O-C)	1116

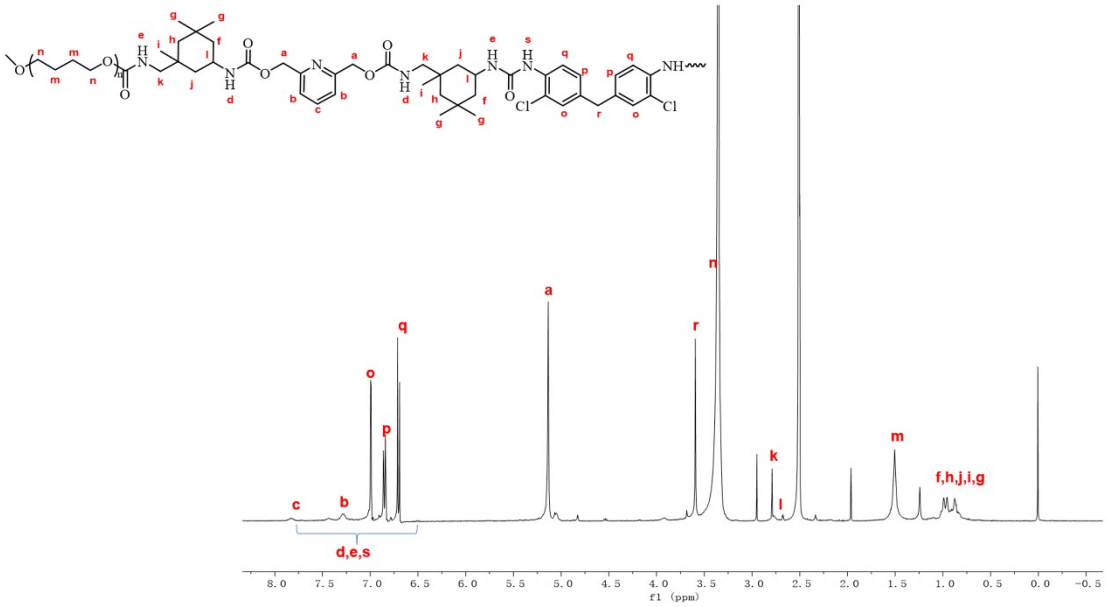

Figure S3. ^{1}HNMR spectrum of $PU_{3.8\text{-}80/20}$.

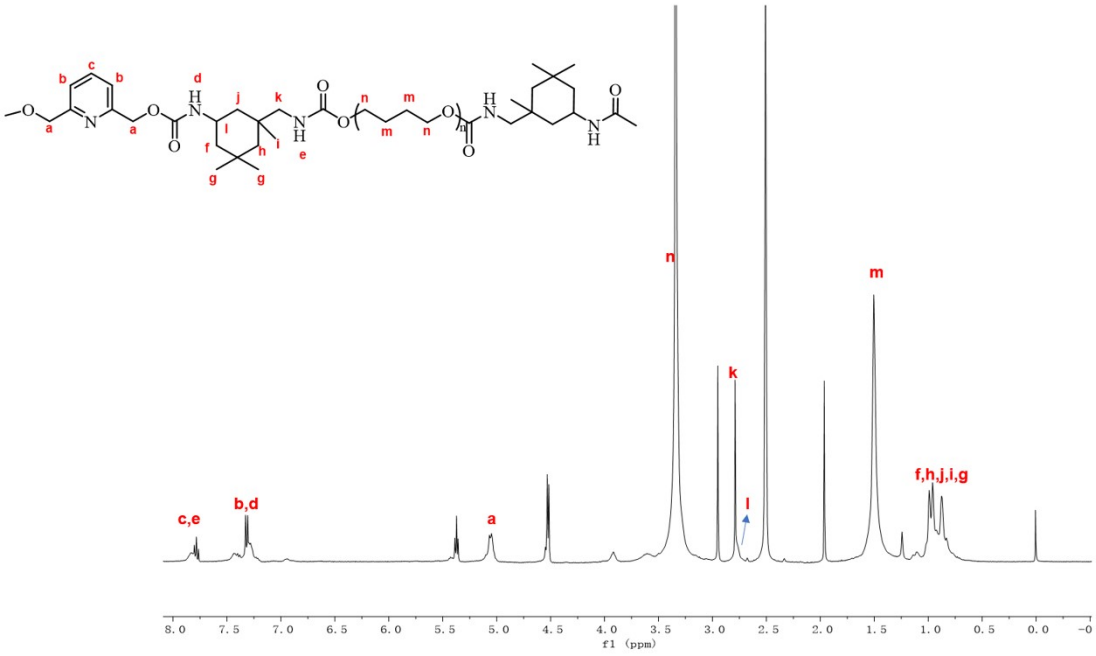

Figure S4. ^{1}HNMR spectrum of $PU_{3.8\text{-}100/0}$.

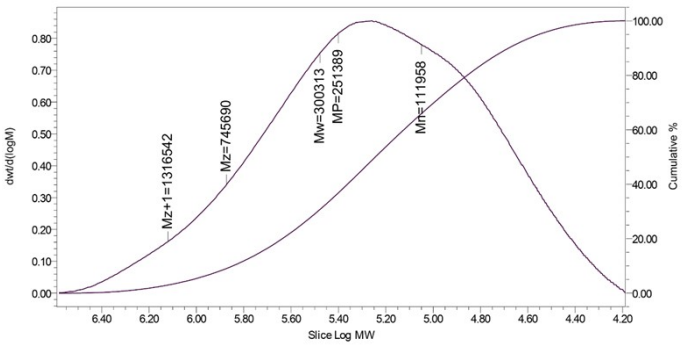
Mz+1=1316542
Mz=745690
Mw=300313
MP=251389
Mn=111958
dwt/d(logM)
Cumulative %
Slice Log MW

(a)

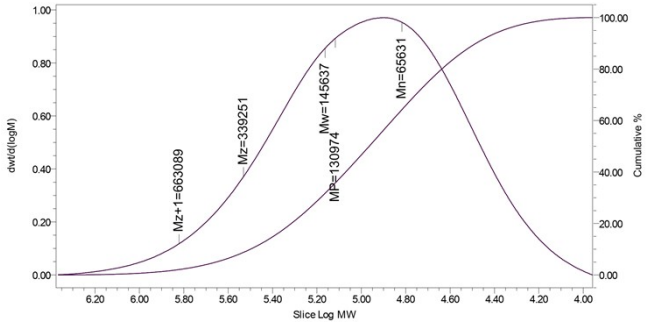
Mz+1=663089
Mz=339251
Mw=145637
MP=130974
Mn=65631
dwt/d(logM)
Cumulative %
Slice Log MW

(b)

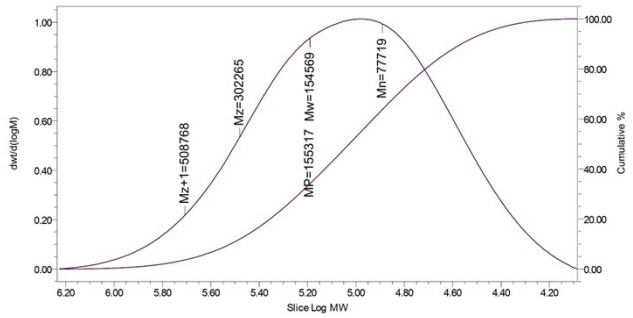
Mz+1=508768
Mz=302265
Mw=154569
MP=155317
Mn=77719
dwt/d(logM)
Cumulative %
Slice Log MW

(c)

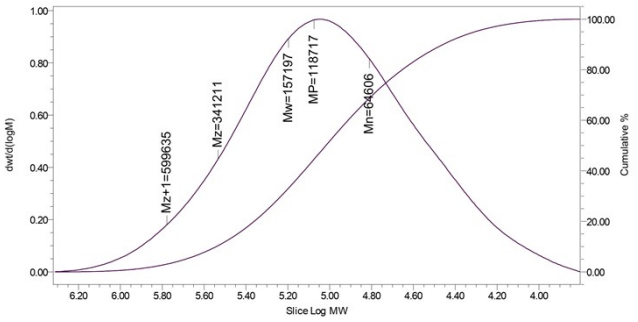
Mz+1=599635
Mz=341211
Mw=157197
MP=118717
Mn=64606
dwt/d(logM)
Cumulative %
Slice Log MW

(d)

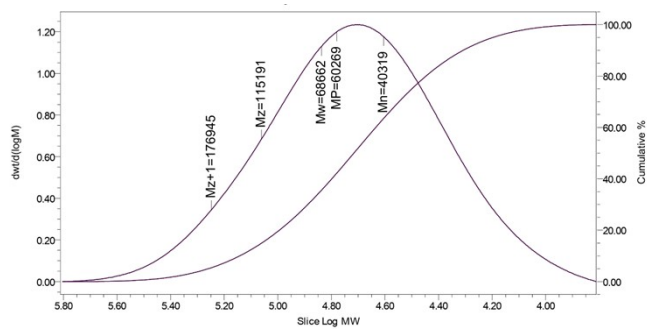

(e)

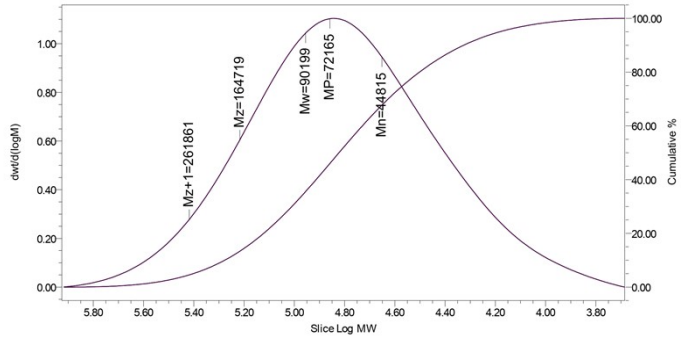

(f)

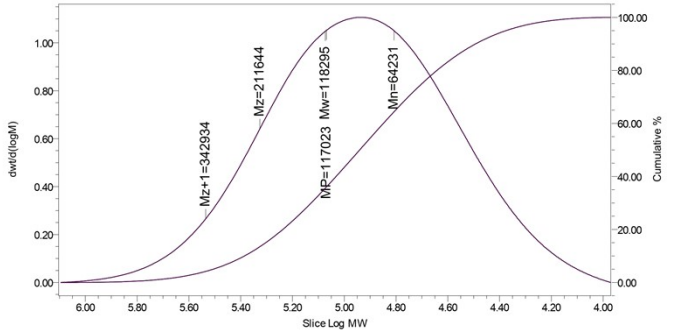

(g)

Figure S5. THF-GPC profiles of PU elastomers. (a) THF-GPC profiles of $PU_{3.0\text{-}80/20}$. (b) THF-GPC profiles of $PU_{3.5\text{-}80/20}$. (c) THF-GPC profiles of $PU_{3.8\text{-}80/200}$. (a) THF-GPC profiles of $PU_{4.0\text{-}80/20}$. (a) THF-GPC profiles of $PU_{3.8\text{-}100/0}$. (a) THF-GPC profiles of $PU_{3.8\text{-}90/10}$. (a) THF-GPC profiles of $PU_{3.8\text{-}70/30}$.

Table S3. The GPC results of PU elastomer.

Sample	M_n(g/mol)	M_w(g/mol)	PDI
$PU_{3.0\text{-}80/20}$	111958	300313	2.483
$PU_{3.5\text{-}80/20}$	65631	145637	2.329
$PU_{3.8\text{-}80/20}$	77719	154569	1.955
$PU_{4.0\text{-}80/20}$	64606	157197	2.171
$PU_{3.8\text{-}100/0}$	40319	68662	1.677
$PU_{3.8\text{-}90/10}$	44815	90199	1.826
$PU_{3.8\text{-}70/30}$	64231	118295	1.789

Table S4. Comparison of mechanical properties and self-healing efficiencies between $PU_{3.8\text{-}80/20}$ and recently reported room-temperature self-healing materials.

Sample source	Tensile strength / MPa	Strain at break / %	Toughness / $MJ.m^{-3}$	Self-healing efficiency /%	Fracture energy / $kJ.m^{-2}$
This work	34.1	2014	127.3	83%	119.1
Ref. 5	1.1	229	6.5	92.9%	---
Ref. 7	16.08	771	75.6	94%	---
Ref. 8	5.72	1726	24.45	61.9%	---
Ref. 13	0.5	1000	---	95	---
Ref. 15	19.47	1144.3	105.2	75%	41.8
Ref. 16	4.83	2010	65.49	98%	42.65
Ref. 17	27.4	770	110	96	---
Ref. 18	1.3	2100	---	97	---
Ref. 25	6.31	710	---	91.6	---
Ref. 26	3.9	348.57	---	76	---
Ref. 28	11.91	723.57	30.07	50	---
Ref. 29	11	725.5	52.1	83	---
Ref. 30	4.2	954	---	90	---
Ref. 31	29	1800	121.8	80%	104.1
Ref. 38	30	700	---	82.27	---
Ref. 39	11.71	295	---	52.6	---
Ref. 40	19.5	675	---	83	---
Ref. 41	3.85	3000	84.02	70	---
Ref. 42	6.8	920	26.9	75	---
Ref. 43	16.1	771	---	94	---
Ref. 44	12.7	182	---	87.3	---

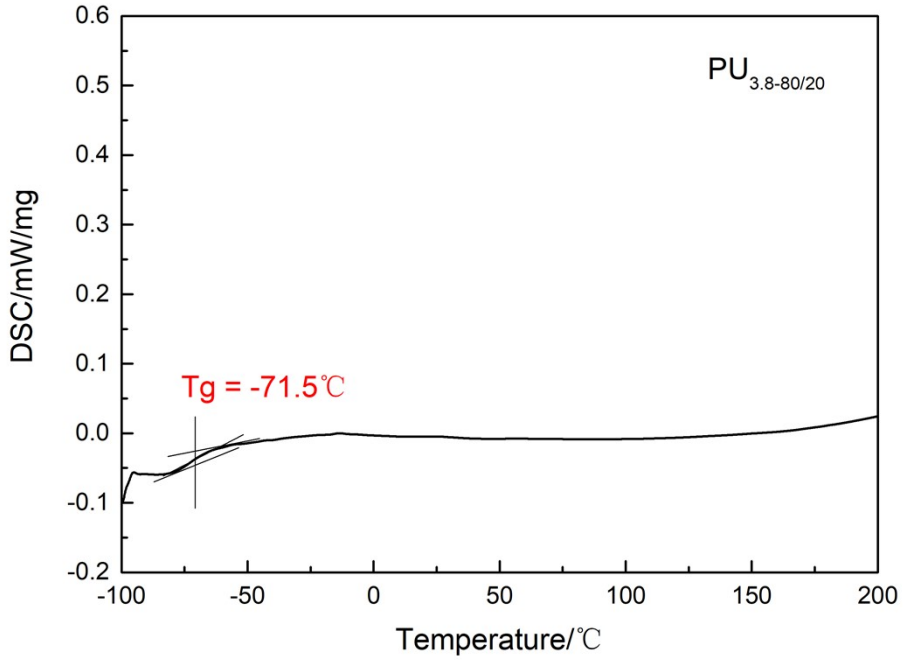

Figure S6. DSC curve of $PU_{3.8\text{-}80/20}$.

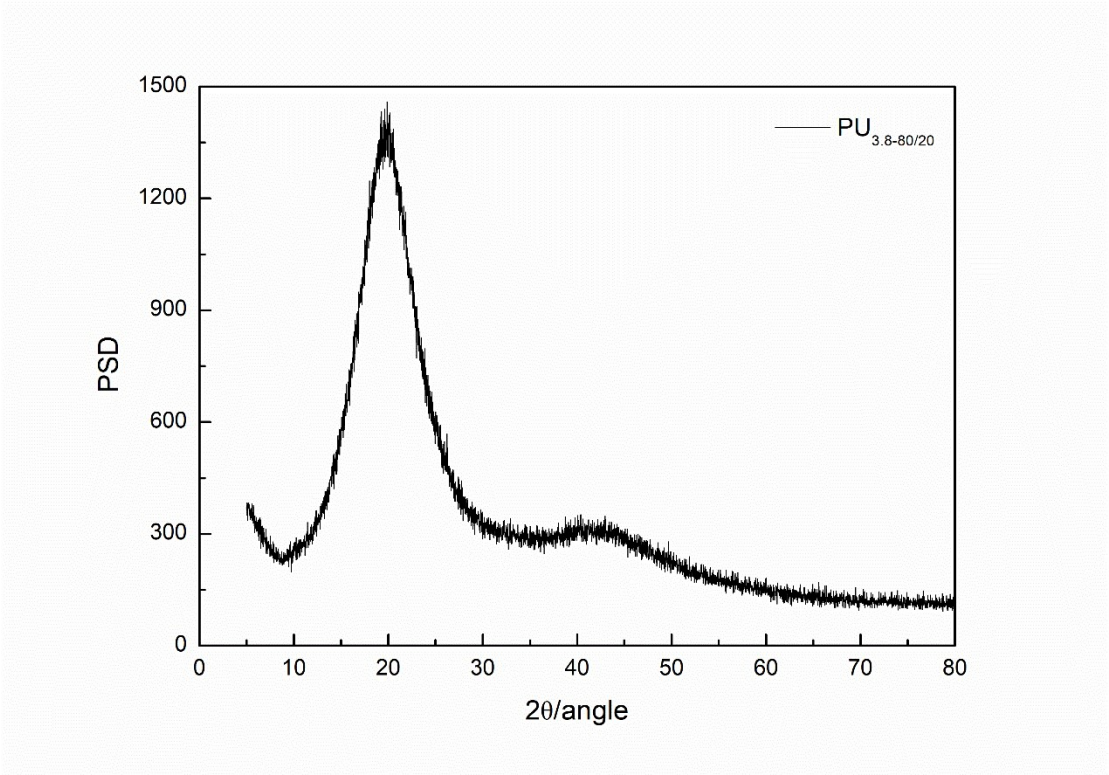

Figure S7. WXAD curve of $PU_{3.8\text{-}80/20}$, the XRD curve only displayed broad diffraction peaks, indicating the amorphous state at room temperature.

Table S5. The original mechanical performances of PU elastomers.

Sample	Tensile strength/MPa	Elongation/%	Toughness/MJ·m^{-3}
$PU_{3.0\text{-}80/20}$	8.4	1855	47.7
$PU_{3.5\text{-}80/20}$	21.6	2309	81.4
$PU_{3.8\text{-}80/20}$	34.1	2014	127.3
$PU_{4.0\text{-}80/20}$	22.2	2481	120.8
$PU_{3.8\text{-}100/0}$	0.6	2960	15.5
$PU_{3.8\text{-}90/10}$	2.0	3003	27.6
$PU_{3.8\text{-}70/30}$	27.5	1806	94.0

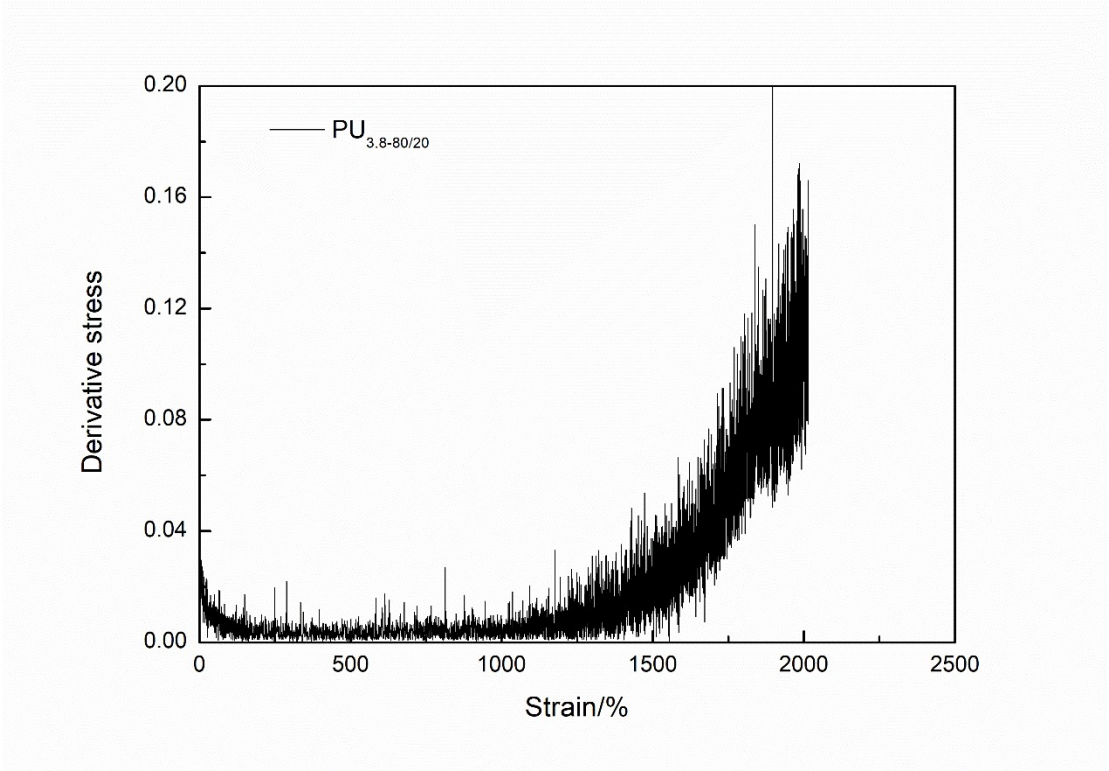

Figure S8. Derivative stress versus strain curve of $PU_{3.8\text{-}80/20}$ for illustrating the changing rate of tensile strength.

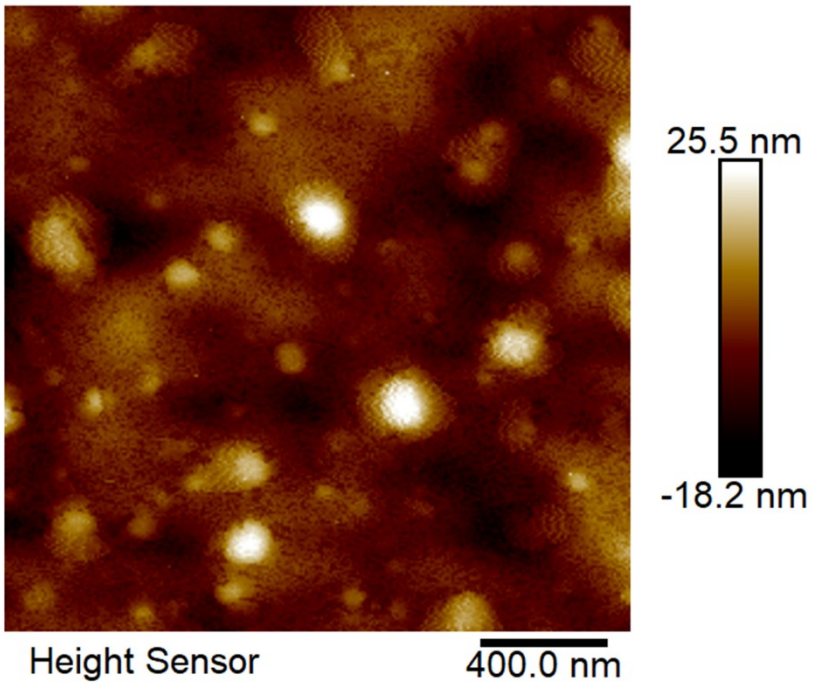

(a)

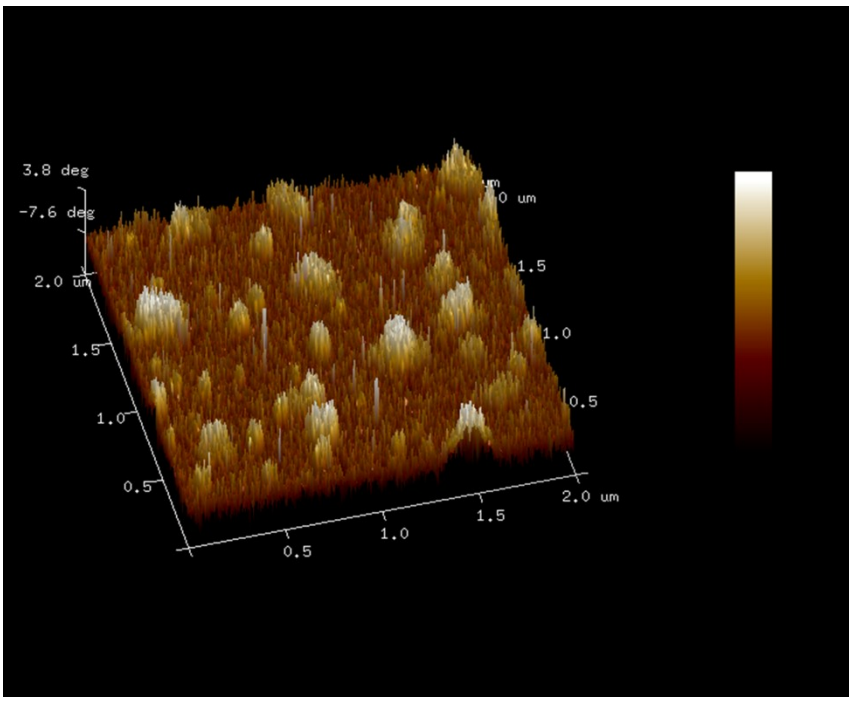

(b)

Figure S9. AFM images of $PU_{3.8\text{-}80/20}$. (a) AFM height sensor image of $PU_{3.8\text{-}80/20}$. (b) AFM 3D phase image of $PU_{3.8\text{-}80/20}$.

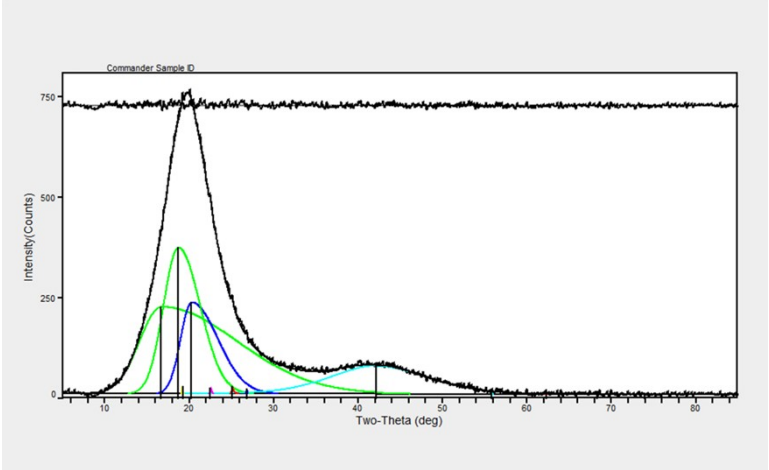
Commander Sample ID
Intensity(Counts)
Two-Theta (deg)

(a)

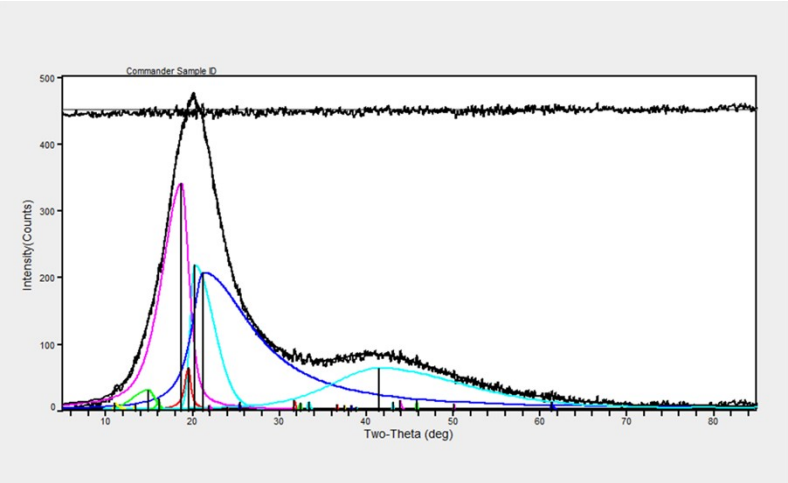
Commander Sample ID
Intensity(Counts)
Two-Theta (deg)

(b)

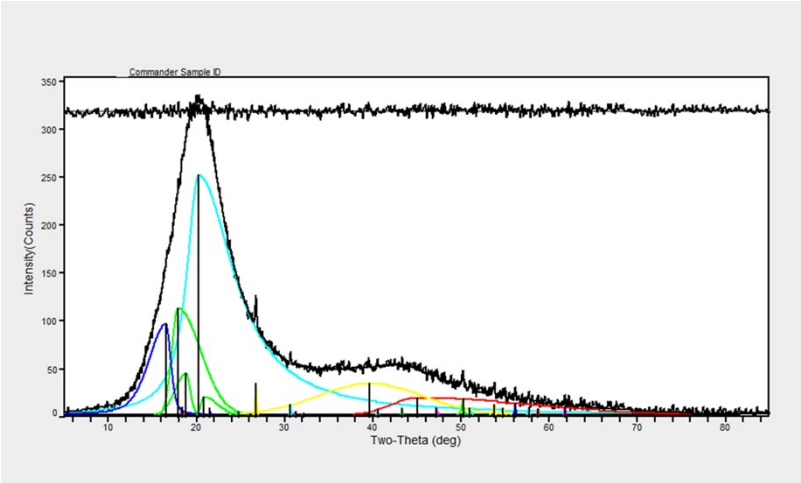
Commander Sample ID
Intensity(Counts)
Two-Theta (deg)

(c)

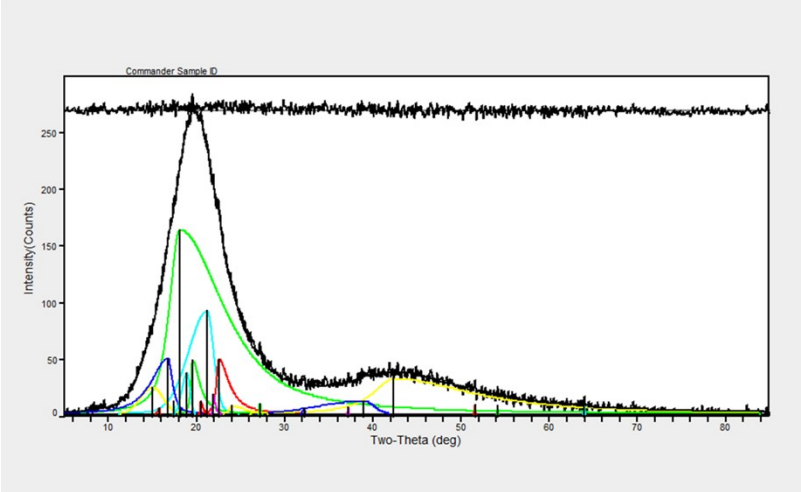

(d)

Figure S10. Fitting calculation (MDI Jade 6 software) of the crystallinity of elastomer $PU_{3.8\text{-}80/20}$ in different strain state. (a) Fitting calculation (MDI Jade 6 software) of the crystallinity of elastomer $PU_{3.8\text{-}80/20}$ in strain state 0%. (b) Fitting calculation (MDI Jade 6 software) of the crystallinity of elastomer $PU_{3.8\text{-}80/20}$ in strain state 500%. (c) Fitting calculation (MDI Jade 6 software) of the crystallinity of elastomer $PU_{3.8\text{-}80/20}$ in strain state 1000%. (d) Fitting calculation (MDI Jade 6 software) of the crystallinity of elastomer $PU_{3.8\text{-}80/20}$ in strain state 1500%.

Table S6. The room-temperature self-healing result of PU elastomer at 25℃ for 48h.

Sample	Tensile strength (SE)/%	Elongation (SE)/%	Toughness (SE)/%
$PU_{3.0\text{-}80/20}$	94.7	91.3	94.6
$PU_{3.5\text{-}80/20}$	88.2	108.8	98.2
$PU_{3.8\text{-}80/20}$	83.3	100.1	88.4
$PU_{4.0\text{-}80/20}$	76.4	101.1	82.0
$PU_{3.8\text{-}100/0}$	98.7	101.2	99.2
$PU_{3.8\text{-}90/10}$	97.0	93.1	96.2
$PU_{3.8\text{-}70/30}$	82.8	99.3	90.7

Table S7. The mechanical performances of $PU_{3.8\text{-}80/20}$ with self-healing time from 12h to 48h.

$PU_{3.8\text{-}80/20}$	Tensile strength (SE)/%	Elongation (SE)/%	Toughness (SE)/%
12h	43.6	78.8	45.9
24h	68.1	90.4	66.7
36h	77.1	94.3	80.1
48h	83.3	100.1	88.4

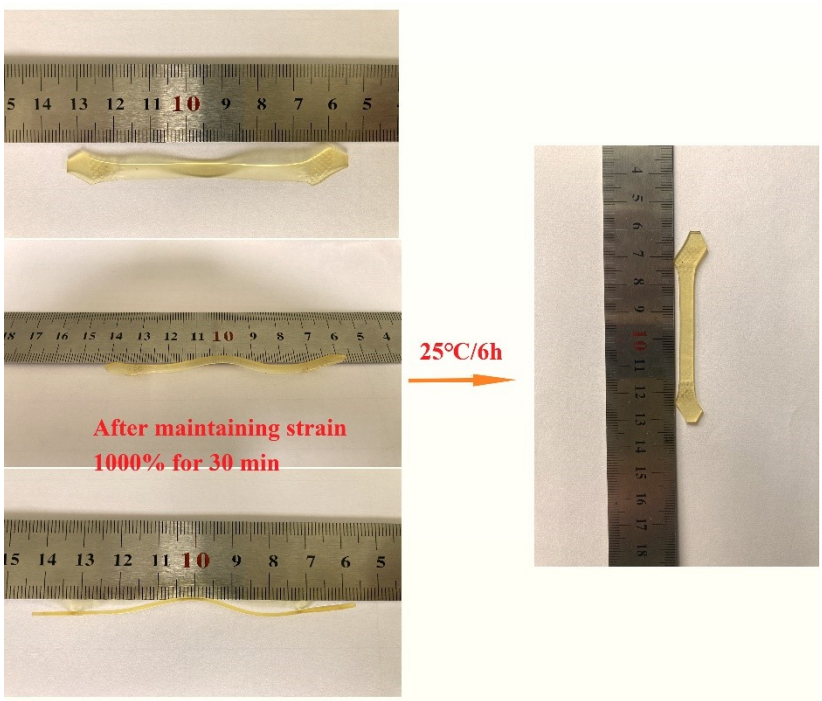

Figure S11. Optical images for after stretching and recovery of $PU_{3.8\text{-}80/20}$ film.

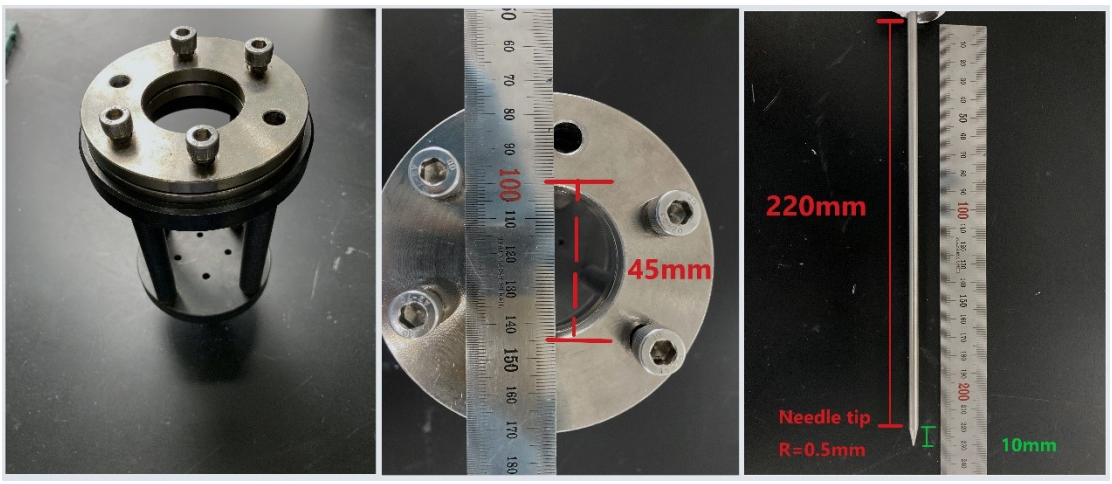

Figure S12. The dimension of steel needle and fixture in puncture test.

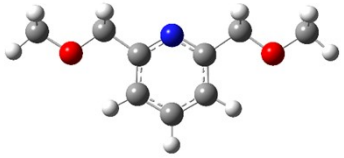

(a)

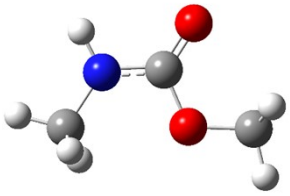

(b)

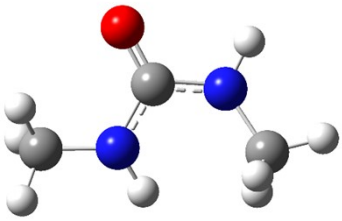

(c)

Figure S13. Optimized molecular structure for simulation. (a) Monomer A. (b) Monomer B. (c) Monomer C.

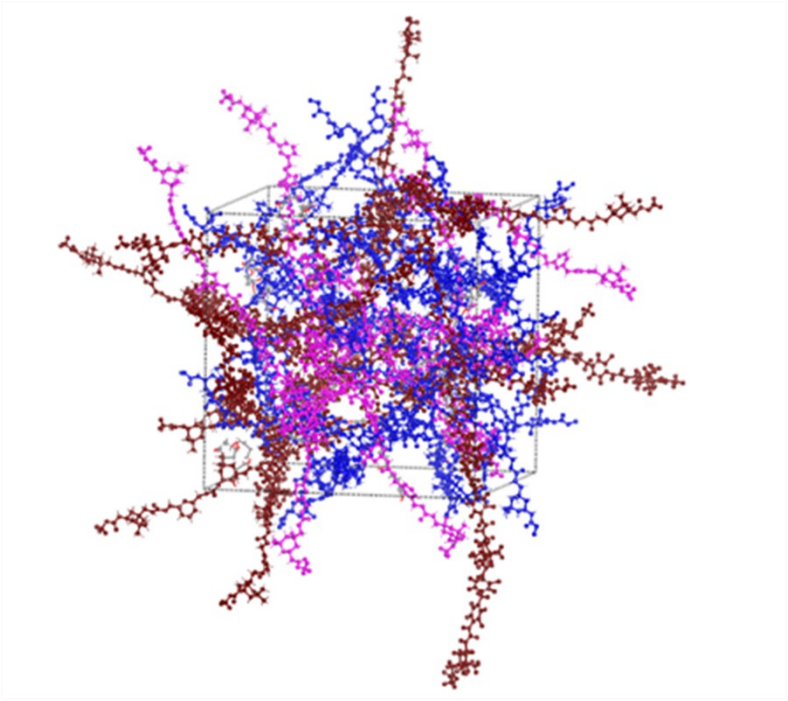

(a)

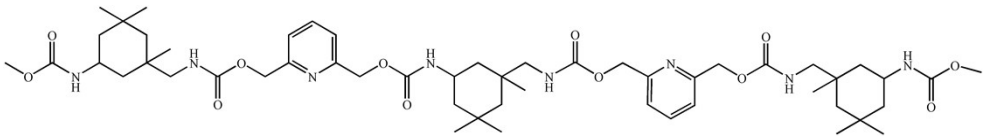

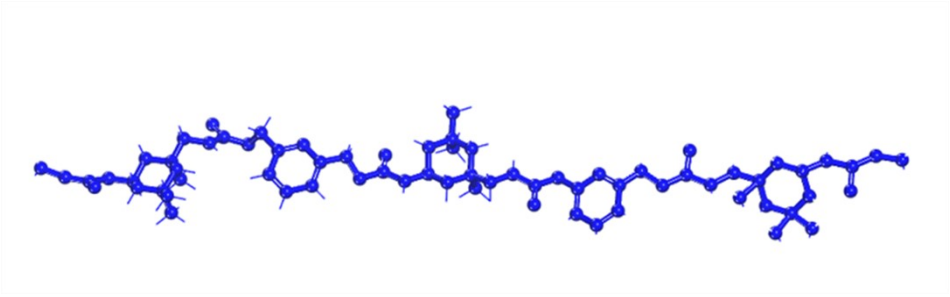

(b)

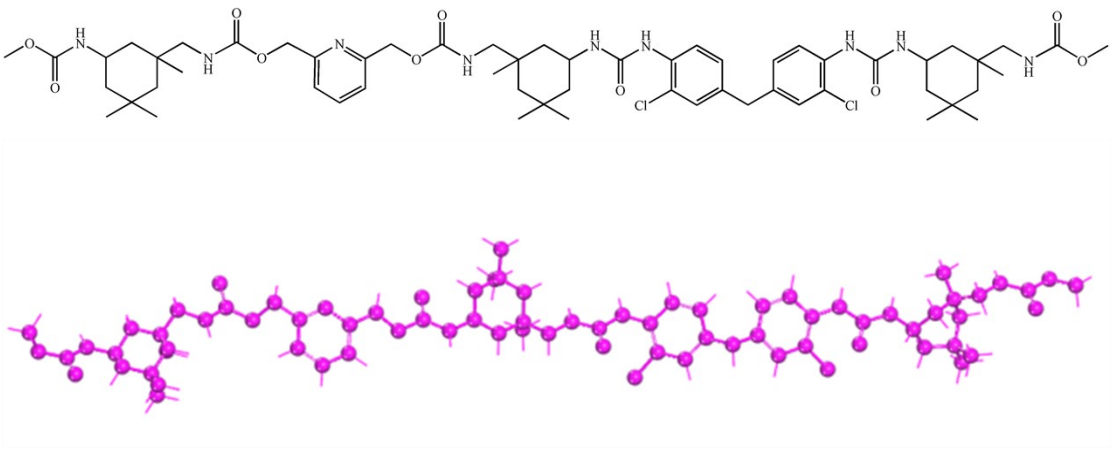

(c)

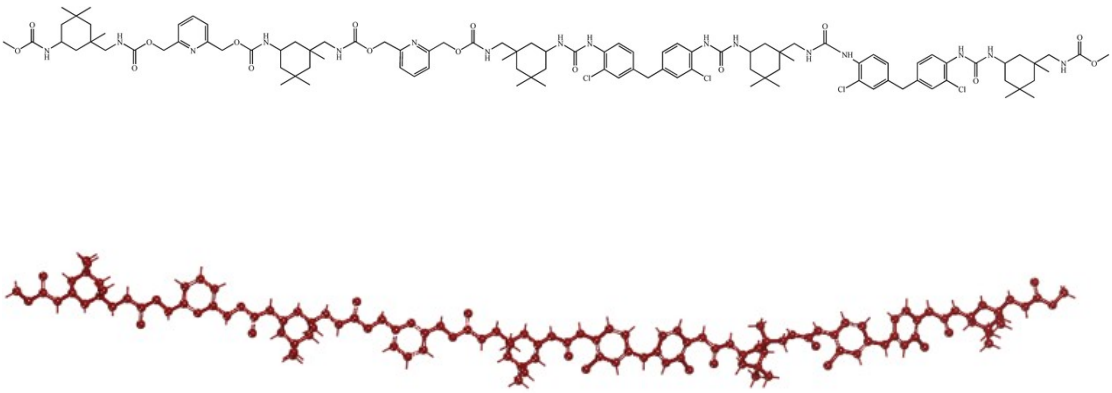

(d)

Figure S14. Schematic representation of a simulated molecular cell of $PU_{3.8\text{-}80/20}$ in the equilibrium state. (a) hard domains are emphasized on the ball-and-stick models. (b) Quantum chemical simulation of hard domains. Optimized hard segments a for simulations. (c) Quantum chemical simulation of hard domains. Optimized hard segments b for simulations. (d) Quantum chemical simulation of hard domains. Optimized hard segments c for simulations.

Quantum chemistry calculation

All calculations in this work were performed using Gaussian 09 program package[1]. Full geometry optimizations were performed to locate all the stationary points, using B3LYP-D3[2]/6-311+G (d, p)[3-4]. Single point energies were also obtained for all optimized structures using dispersion-corrected density functional (DFT-D3(BJ)) with the 6-311+G (d, p) basis set. Quantumtheory of atoms-in-molecules (QTAIM) descriptors and other H-Bondongs were calculated based on high-quality density functional theory wave functions using the Multiwfn software[5]. The monomer structures A, B, C were illustrated in Figure S13.

Molecular simulation method

Molecular dynamic simulations were performed to study the polymer behavior. Our simulation calculation was conducted on four structures with an integration time-step of 1 fs. Periodic boundary conditions were applied in the *x*- and *y*-dimensions. The box size of the samples was 50 × 50 ×50 nm^3 (Figure S14 a). First, the conjugate gradient algorithm and energy minimization were performed to obtain a stable structure. Condensed-phased Optimized Molecular Potential for Atomistic Simulation Studies force field was also used to optimize these structures. Each sample was then equilibrated under the NPT ensemble at a constant temperature of 300 K to achieve an equilibrium state with zero pressure for 30 ns. The equilibration molecular systems of the pure separation membrane could be obtained after geometrically optimizing. The system is composed of 30 a, 10 b, 10 c (Figures S14 b, c, d), and 10 soft segments. Furthermore, a potential cutoff radius of 2.25 nm is applied in the calculation of the non-bonded interaction. And the PPPM has been used to describe the electrostatic. The Andersen feedback thermostat and Berendsen barostat algorithm are applied in the system with temperature and pressure conversion. Finally, the properties of our structures are obtained in the last 3000 ps. The binding energy can be used to measure the intensity of the interaction between a, b and c.

Reference

1. M.J. Frisch, G.W. Trucks, H.B. Schlegel, G.E. Scuseria, M.A. Robb, J.R. Cheeseman, G. Scalmani, V. Barone, B. Mennucci, G.A. Petersson, H. Nakatsuji, M. Caricato, X. Li, H.P. Hratchian, A.F. Izmaylov, J. Bloino, G. Zheng, J.L. Sonnenberg, M. Hada, M. Ehara, K. Toyota, R. Fukuda, J. Hasegawa, M. Ishida, T. Nakajima, Y. Honda, O. Kitao, H. Nakai, T. Vreven, J.A. Montgomery, J.J.E. Peralta, F. Ogliaro, M. Bearpark, J.J. Heyd, E. Brothers, K.N. Kudin, V.N. Taroverov, T. Keith, R. Kobayashi, J. Normand, K. Raghavachari, A. Rendell, J.C. Burant, S.S. Iyengar, J. Tomasi, M. Cossi, N. Rega, J.M. Millam, M. Klene, J.E. Knox, J.B. Cross, V. Bakken, C. Adamo, J. Jaramillo, R. Gomperts, R.E. Stratmann, O. Yazyev, A. J. Austin, R. Cammi, C. Pomelli, J. W. Ochterski, R.L. Martin, K. Morokuma, V.G. Zakrzewski, G.A. Voth, P. Salvador, J.J. Dannenberg, S. Dapprich, A.D. Daniels, O. Farkas, J.B. Foresman, J.V. Ortiz, J. Cioslowski, D.J. Fox, Gaussian 09 (Revision D.01), I. Gaussian, Wallingford, CT, **2013**.

2. Grimme, S.; Antony, J.; Ehrlich, S.; Krieg, H., A consistent and accurate ab initio parametrization of density functional dispersion correction (DFT-D) for the 94 elements H-Pu. *J. Chem. Phys.* **2010,** *132* (15), 154104.

3. Xu S., He T., Li J., Huang Z., & Hu C., Enantioselective synthesis of D-lactic acid via chemocatalysis using MgO: Experimental and molecular-based rationalization of the triose's reactivity and preliminary insights with raw biomass. *Appl. Catal. B: Environ.* **2021**, 292:120145.

4. McLean, A. D.; Chandler, G. S. Contracted Gaussian basis sets for molecular calculations. I. Second row atoms, Z = 11−18. *J. Chem. Phys.* **1980**, 72, 5639−5648.

5 Lu, T.; Chen, F., Multiwfn: a multifunctional wavefunction analyzer. *J. Comput. Chem.* **2012,** *33* (5), 580-92.